11-1-2023

All dielectric highly efficient achromatic meta-lens using inverse design optimization

Abdullah Maher

Mohamed A. Swillam

All dielectric highly efficient achromatic meta-lens using inverse Design Optimization

Abdullah Maher
The American University in Cairo
Mohamed A. Swillam (m.swillam@aucegypt.edu)
The American University in Cairo

Article

Keywords:

Posted Date: August 4th, 2023

DOI: https://doi.org/10.21203/rs.3.rs-3206824/v1

Additional Declarations: No competing interests reported.

Version of Record: A version of this preprint was published at Scientific Reports on November 1st, 2023.
See the published version at https://doi.org/10.1038/s41598-023-45231-y.

All dielectric highly efficient achromatic meta-lens using inverse Design Optimization

Abdullah Maher[1], **Mohamed A. Swillam**[1,*]

[1]Department of Physics, The American University in Cairo, 11835, New Cairo, Egypt

[*]m.swillam@aucegypt.edu

ABSTRACT

This work presents a high-efficiency achromatic meta-lens based on inverse design with topology optimization methodology. The meta-lens design with high numerical aperture values (NA = 0.7, NA= 0.8, and NA = 0.9) along the visible band starts from 450 nm to 800 nm. The final optimized structures for the three conditions of the high numerical apertures have high focusing efficiency along the design band. The optimization problem is based on Kreisselmeier–Steinhauser (k-s) objective function, leading to approximately stable response over the broadband bandwidths of the three designs.

Introduction

Photonics devices are becoming a significant aspect of future technology since it relates to the synthesis, manipulation, and detection of light related to practical applications where the polarity of the light is vital [1]-[3]. It's a major potential for designing and manufacturing devices, systems, and integrated circuits for applications in high-speed data transmission, enhancing sensing and imaging photonic technology promises orders of magnitude speed gains while consuming less power [4]-[7]. The optical performance of the photonics device is accessible by sweeping all the possible solutions where the higher order of the degree of freedom (DOF) requires a large simulation time, so the interest in satisfactory results and simulation time efficiency inverse design methodology employed, which depended mainly on the iterative optimization algorithms. In principle, the inverse design approaches require a clear definition of the objective function and the design of constraints. These constraints can be related to fabrication limitations, cost, and total footprint. The formulation of these parameters as an optimization problem is performed to achieve the optimal solution and the required optimal parameters [8]-[10]. The first one is shape optimization [11] which starts with a suitable guess and perturbs the boundaries such that some figures of merit (FOM) are optimized. The second one is called the topology optimization, [12]-[14] which continuously varies the geometry yielding on optimal topology and shape that achieve the some FOM. In our work, we use inverse design with topology optimization to design a high-efficiency optical element, and our work relies on significant optical element meta-lens [15]. Meta-lens technology is gaining popularity due to its numerous uses in many applications [7][16] such as polarization imaging systems, phase imaging systems, light field cameras, and solar energy harvesting. In the case of designing conventional or traditional meta-lens, there are two methods for dispersion elimination. The first method is called the panchayat man-berry phase (geometric phase) [17] by changing the orientation of the meta-unit where the geometric phase operates under circularly polarized incidence. The second one is by controlling the resonance of the generally fluctuating [15]. The meta-lens based on the two designed is efficient in case of simple functionality in a single wavelength, but in many cases with complex functionality the forward or conventional design is not efficient such as the high efficiency under the high numerical aperture (NA) value [14], in such this design and optimization challenge an inverse solution would be far more adept, so we use inverse design with topology optimization to produce broadband focusing efficiency with high NA meta-lens [18][19]. We demonstrated three designs based on three high numerical aperture conditions (NA= 0.7, NA = 0.8, and NA = 0.9) by observing the results with some parameters such as focusing efficiency, full-width half maximum (FWHM) and the field distribution along the design simulation area. Despite there is previous work studied the focusing efficiency of the meta-lens under high numerical aperture conditions [14], The meta-lens design presented in this paper under the three numerical aperture conditions optimized along the wavelength band 350 nm starting from 450 nm to 800 nm, but in the results section, we extend the range from 400 nm to 1200 nm based on a direct FEM solver. Due to the number of constraints (wavelengths) in the optimization problem, we need to reduce it by aggregation objective function. A maximum or a minimum value function is an obvious choice for these constraints aggregated, but both functions are not differentiable and inefficiently integrated with gradient-based design optimization, so the optimization problem depends on smooth estimators called the Kreisselmeier–Steinhauser (k-s) [20]. In gradient-based optimization, the k-s is an extensively used constraints aggregation methodology and has been applied in many applications, especially in civil construction design optimization [21]. In our design, the formulation of the optimization problem for the inverse design band from 450 nm to 800 nm depends on the Kreisselmeier–Steinhauser (k-s) objective function, where it targets 350 nm along the wavelengths band, but the design challenge in the topology optimization is related to the limitation of the spatial oscillation of

the design field, so the design field is applied to the standard filtering and thresholding Heaviside function to recover between the two design materials. Titanium dioxide (Tio_2) is selected for all meta-lens design because it's optically clear in the design band (400 nm: 1200nm) and has excellent manufacturability in the nanoscale. Finally, the focusing efficiency of the meta-lens along the optimization band (450 nm: 800 nm) for the three numerical aperture conditions reaches a maximum value of 70%, 56.54%, and 48.67% for NA values 0.7, 0.8, and 0.9, respectively and the final optimized structure for the three designs are suitable for the fabrication process.

Methods

Working principle. The Fig. 1 shows the boundaries Γ which subjected to the first order absorbing boundary conditions.

$$n\nabla E_z(r) = -ikE_2(r),\ r \in \Omega. \tag{1}$$

where n denotes the surface normal and i the imaginary unit. The model in fig.1 represents the meta-lens design consisting of the model domain Ω of height h_Ω, which consists of substrate height h_s, optimized region height $h_{\Omega D}$, and remained height for air. The simulation width is w_Ω, and the design width is $w_{\Omega D}$. The focus point is r_p which is determined then the field strength is determined to obtain the objective function Φ, called the figure of merit (FOM). All dimensions of the design in fig.1 are listed in table.1. The models are discretized by finite element method (FEM) [12].

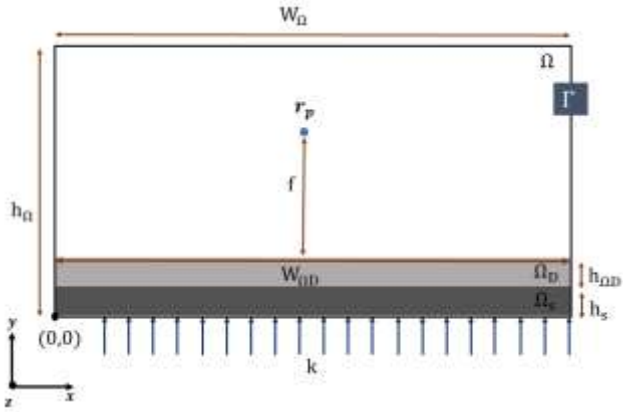

Figure1. The meta-lens design and the boundary condition.

h_Ω	w_Ω	$w_{\Omega D}$	$h_{\Omega D}$	h_s
$8\ \mu m$	$6\ \mu m$	$6\ \mu m$	$0.25\ \mu m$	$0.25\ \mu m$

Table1. Values for Quantities in Fig.1.

The focal length f and the focus point r_p depending mainly on the numerical aperture condition [13], and numerical aperture of the meta-lens can be calculated from:

$$\mathrm{NA} = \sin\left(\arctan\left(\frac{w_{\Omega_D}}{2f}\right)\right), \tag{2}$$

Where the values of f respected to the NA conditions are observed in table.2.

NA	0.7	0.8	0.9
f	$3\ \mu m$	$2.1\ \mu m$	$1.4\ \mu m$

Table2. The values of f respected to the NA condition.

Material interpolation algorithms are used in density-based topology optimization to relate a change in the design field to a change in the local spatial material property in the physical model problem [22]. The relation between refractive index η, extinction coefficient k, and electric permittivity ε_r is given by:

$$\varepsilon_r = (\eta^2 - k^2) - 2i\eta k\,. \tag{3}$$

To formulate the non-linear interpolation scheme [22]:

$$\begin{aligned} \epsilon_r(\eta(\rho),\kappa(\rho)) &= (\eta(\rho)^2 - \kappa(\rho)^2) - \mathrm{i}(2\eta(\rho)\kappa(\rho)) \\ \eta(\rho) &= \eta_{\mathrm{M}_1} + \rho\left(\eta_{\mathrm{M}_2} - \eta_{\mathrm{M}_1}\right) \\ \kappa(\rho) &= \kappa_{\mathrm{M}_1} + \rho\left(\kappa_{\mathrm{M}_2} - \kappa_{\mathrm{M}_1}\right). \end{aligned} \tag{4}$$

Where M_1 and M_2 denotes the two materials being interpolated, the interpolation parameters ρ is varying from zero to one to relate between the two materials. The design is based on all Tio2 material as a high index material, and it's interpolated with air as low index material. The measured data of the refractive index (η) and the extinction coefficient (κ) of the Tio2 that we depended on [23] are shown in fig.2(a) and fig.2(b), respectively.

(a)

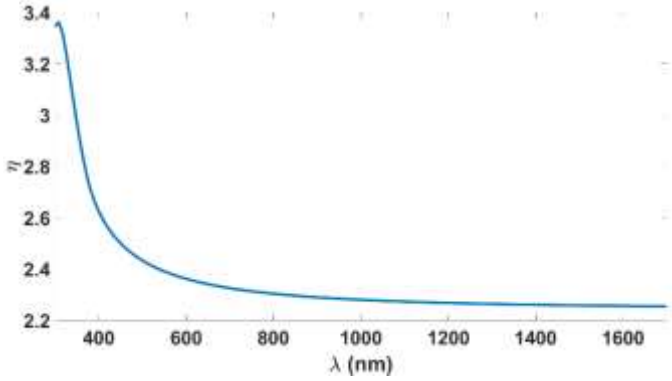

(b)

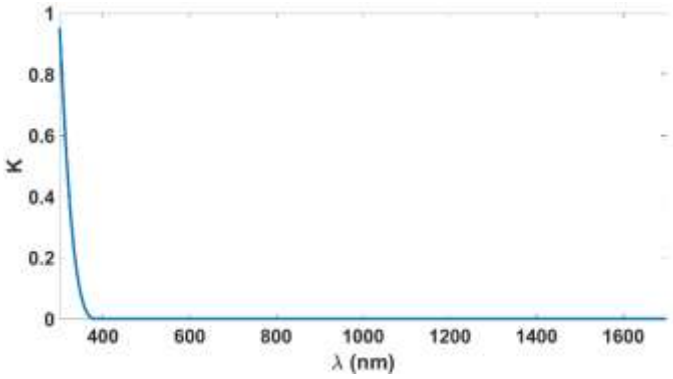

Figure2. (a) The refractive index of Tio2; **(b)** The extinction coefficient of Tio2.

The figure of merit ϕ as a function of the magnitude $|E|^2$ at the focal point r_p is**:**

$$\phi\left(\rho(r), r_p\right) = \left|E_z\left(\rho(r), r_p\right)\right|^2 = E_z\left(\rho(r), r_p\right)^* E_z\left(\rho(r), r_p\right). \tag{5}$$

The optimization problem (eq.9) based on The Kreisselmeier–Steinhauser (k-s) [20] objective function targets 350 nm of wavelength range simultaneously with the number of points ($N_\lambda = 40$). The k-s aggregation function is an alternative differentiable function to the max-mini function where the value of p overestimates the constraints minimum [20]. The formulation of FOM based on the k-s objective function can be written as:

$$\Phi_{k-S} = \frac{-1}{p}\ln\left(\sum_{i=1}^{N_\lambda} e^{-p\left(\Phi_i\left(E_z\left(\lambda_i, r_P, \varepsilon_r(\rho(r),\lambda_i)\right)\right)\right)}\right). \tag{6}$$

The equality constraints of the optimization problem [12][13] are related to the operator ℓ_{EM} , where the operator denotes applying the effect of the physical system to the state field for the excitation F. The solution to the optimization problem depends mainly on the interpolation parameters $\rho(r)$ to interpolate between the high index material (Tio2) and the low index material (air). To limit the spatial oscillation of the design field a standard filtering is applied to the ρ parameter over Ω_{D} using the equation:

$$-\left(\frac{r_f}{2\sqrt{3}}\right)^2 \nabla\tilde{\rho}(\mathbf{r}) + \tilde{\rho}(\mathbf{r}) = \rho(\mathbf{r})\,, \qquad r_f > 0, \quad r \in \Omega_{\mathrm{D}}. \tag{7}$$

Where the r_f is the filter radius. Then the filter is followed by thresholding using a smoothed approximation of the Heaviside function (eq. 8) to recover a design between the Tio2 material and the background material (Air):

$$\bar{\tilde{\rho}} = \frac{\tanh\left(\beta\cdot\eta\right)+\tanh\left(\beta\cdot(\tilde{\rho}-\eta)\right)}{\tanh\left(\beta\cdot\eta\right)+\tanh\left(\beta\cdot(1-\eta)\right)}, \qquad \beta \in [1,\infty[,\ \eta \in [0,1]. \tag{8}$$

Where β is the threshold strength and η is the threshold level. The algorithm used to solve the design problem is MATLAB's fmincon. The optimization parameters are listed in the table. 3. Where the n_{iter} is the inner iteration taken to solve the optimization problem.

Parameter	η	β	r_f(nm)	n_{iter}	p
Value	0.5	5	60	200	2

Table3. The optimization parameters.

Finally, the optimization problem is formulated as:

$$
\begin{aligned}
&\max_{\rho}\left(\frac{-1}{p}\ln\left(\sum_{\mathrm{i}=1}^{N_2} e^{-p\left(\Phi_{\mathrm{i}}\left(E_{\mathrm{z}}\left(\lambda_{\mathrm{i}},r_p,\varepsilon_r\left(\bar{\tilde{\rho}}(r),\lambda_{\mathrm{i}}\right)\right)\right)\right)}\right)\right)\\
&\text{s.t. } \ell_{EM}\left(E_z(\lambda_{\mathrm{i}},r),\varepsilon_r\left(\bar{\tilde{\rho}}(r),\lambda_{\mathrm{i}}\right)\right)=F(r,\lambda_{\mathrm{i}})\Big)\\
&\varepsilon_r\left(\bar{\tilde{\rho}}(r),\lambda_{\mathrm{i}}\right)=\left(\eta^2\left(\bar{\tilde{\rho}}(r),\lambda_{\mathrm{i}}\right)-k^2\left(\bar{\tilde{\rho}}(r),\lambda_{\mathrm{i}}\right)\right)-2\mathrm{i}\eta\left(\bar{\tilde{\rho}}(r),\lambda_{\mathrm{i}}\right)k\left(\bar{\tilde{\rho}}(r),\lambda_{\mathrm{i}}\right)\Big)\\
&\eta\left(\bar{\tilde{\rho}}(r),\lambda_{\mathrm{i}}\right)=\eta_{M1}(\lambda_{\mathrm{i}})+\rho(r)\left(\eta_{M2}(\lambda_{\mathrm{i}})-\eta_{M1}(\lambda_{\mathrm{i}})\right)\\
&k\left(\bar{\tilde{\rho}}(r),\lambda_{\mathrm{i}}\right)=k_{M1}(\lambda_{\mathrm{i}})+\rho(r)\left(k_{M2}(\lambda_{\mathrm{i}})-k_{M1}(\lambda_{\mathrm{i}})\right)\\
&\bar{\tilde{\rho}}=\frac{\tanh(\beta\cdot\eta)+\tanh(\beta\cdot(\tilde{\rho}-\eta))}{\tanh(\beta\cdot\eta)+\tanh(\beta\cdot(1-\eta))},\\
&-\left(\frac{r_f}{2\sqrt{3}}\right)^2\nabla\tilde{\rho}(\mathbf{r})+\tilde{\rho}(\mathbf{r})=\rho(\mathbf{r})\ ,\\
&0\le\rho(r)\le 1, r\in\Omega_{\mathrm{D}}.
\end{aligned}
\tag{9}
$$

The sensitivity of the k-s aggregation function (eq. 10) respected to the design variable can be written as:

$$
\frac{\partial\Phi_{k-s}(\rho)}{\partial\rho}=\frac{\sum_{i=1}^{N_\lambda} e^{-p(\Phi_i(\rho))}\frac{\partial\Phi_i(\rho)}{\partial\rho}}{\sum_{i=1}^{N_\lambda} e^{-p(\Phi_i(\rho))}}. \tag{10}
$$

The gradient Φ respected to the design variables k ($\bar{\tilde{\rho}}_{\mathrm{k}}$) is derived by the adjoint sensitivity method [12]:

$$
\frac{\partial\Phi}{\partial\bar{\tilde{\rho}}_{\mathrm{k}}}=2\Re\left[\lambda^T\frac{\partial S}{\partial\bar{\tilde{\rho}}_{\mathrm{k}}}E_Z\right]. \tag{11}
$$

where λ is a vector of nodal complex Lagrange multipliers and $\Re$ denotes the real part.

Results

The inverse design range starts from 450 nm to 800 nm. The final optimized structures under the three NA conditions (NA = 0.7, NA =0.8, and NA = 0.9) resulting from the inverse design are solved directly from 400 nm to 1200 nm by the FEM solver. To observe the results of the meta-lens design, we need to define some illustration parameters such as the electric field distribution along the design area (x-y) plane, the full-width half maximum (FWHM), and finally, the focusing efficiency, where it's calculated by the ratio of the power within a spot of diameter equal to 3 times the simulated full-width at half-maximum (FWHM) to the total incident power. For meta-lens under numerical aperture condition (NA = 0.7), the final binary structure is shown in fig.3 where the black represents the high index material (Tio2), and the white represents the low index material (Air). The focusing efficiency as observed in fig.4(a) has a maximum value of 70% along the inverse design band and an average value of 53.56%. For all wavelengths range, the average value of the focusing efficiency is 49.13%, and the minimum value is 11.18%, while the FWHM along the inverse design range in fig.4(b) has a maximum value of 450 nm and an average value of 394.7 nm, but along the full band, it has an average value of 390.15 nm. The normalized field distribution along the simulation area (x-y plane) and the normalized field intensity over the focal plane are shown in fig.5 and fig.6, respectively.

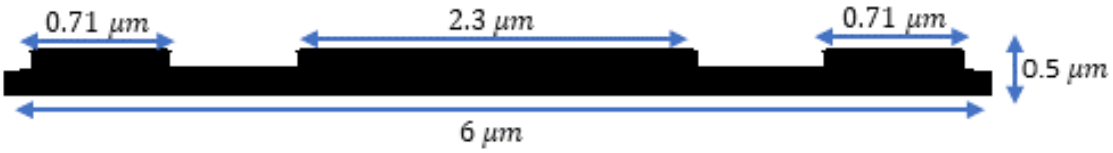

Figure3. The final binary optimized structure of the meta-lens under the numerical aperture condition (NA = 0.7).

(a)

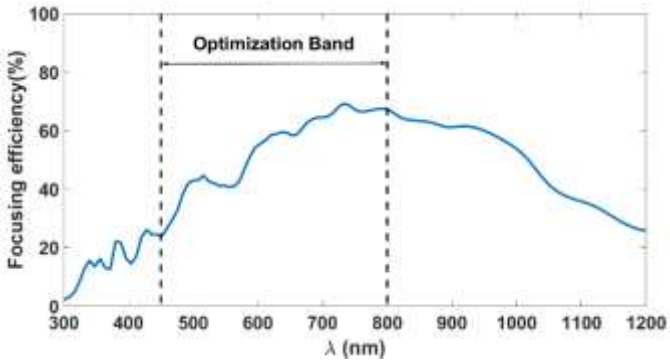

(b)

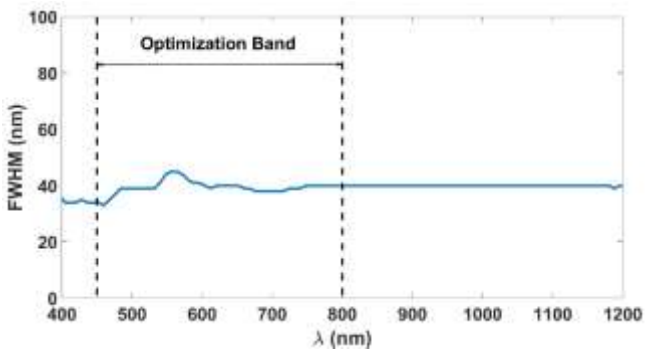

Figure4. (a) Focusing efficiency of meta-lens with NA = 0.7; **(b)** FWHM of meta-lens with NA = 0.7.

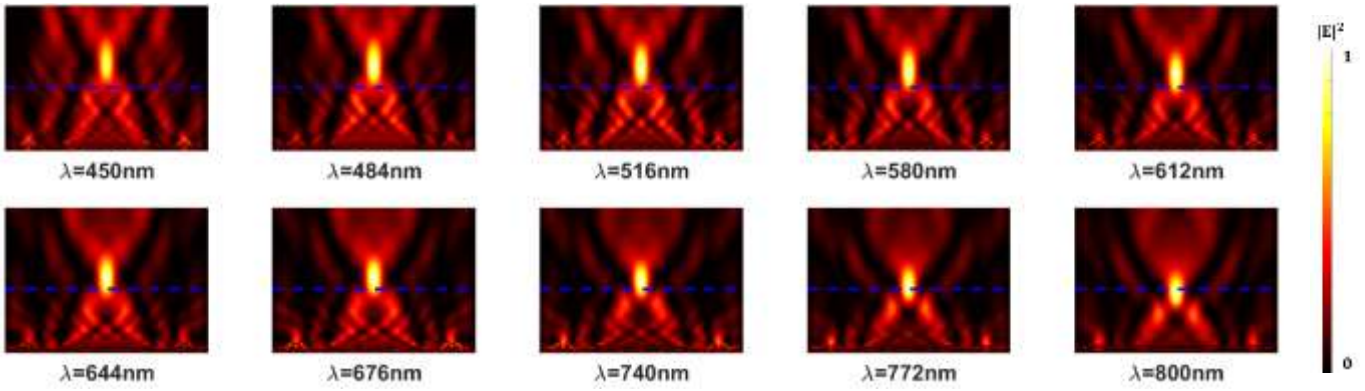

Figure5. The normalized electric field distribution along the simulation area (x-y plane) of the meta-lens with NA =0.7. The blue dashed line represents the focal plane.

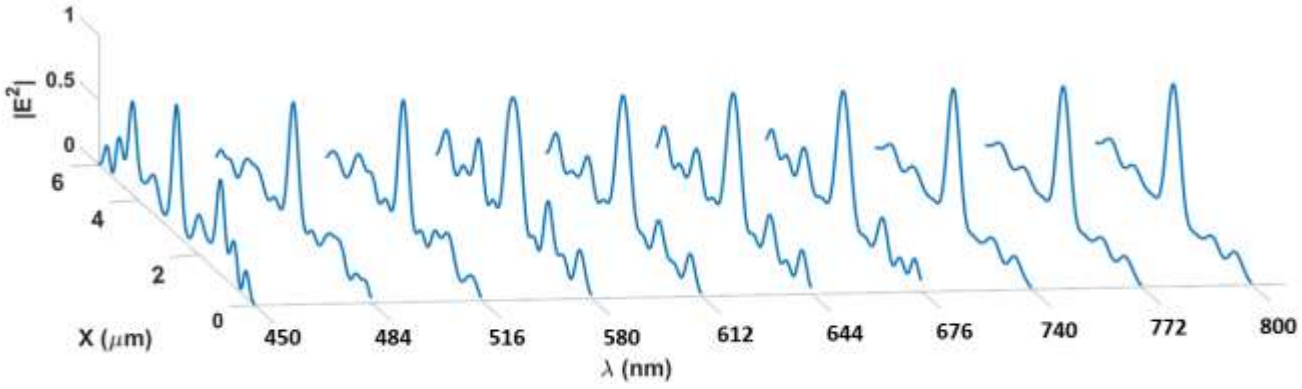

Figure6. The normalized field intensity over the focal plane of the meta-lens with NA = 0.7.

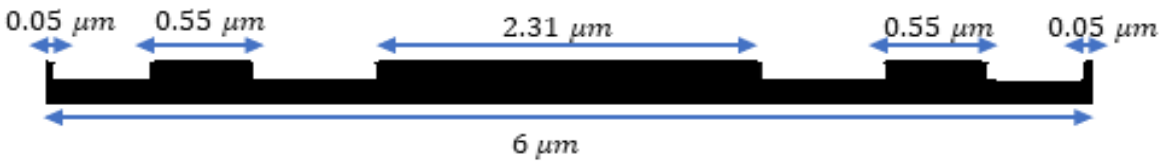

Figure7. The final binary optimized structure of the meta-lens under the numerical aperture condition (NA = 0.8).

In the case of meta-lens with numerical aperture condition (NA = 0.8), the overall wavelength range (400: 1200 nm) has a focusing efficiency as a maximum value of 56.54% at wavelength 700 nm and an average of 29.33% along the whole band(fig.8(a)). In the inverse design band, the focusing efficiency ranges from 16.02% to 56.54% with an average value of 29.33%. The FWHM in fig. 8(b) has a maximum value of 410 nm, an average value of 287.1 nm, and 279.9 nm along the full wavelength range. The final binarized structure is observed in fig. 7, also the electric field distribution and the normalized field intensity are shown in fig. 9 and fig. 10, respectively.

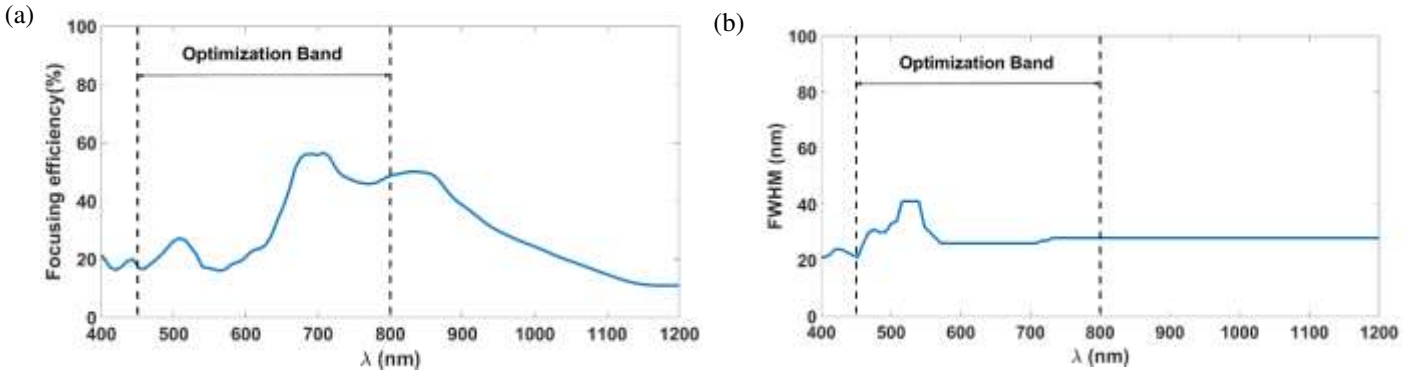

Figure8. (a) Focusing efficiency of meta-lens with NA = 0.8; **(b)** FWHM of meta-lens with NA = 0.8.

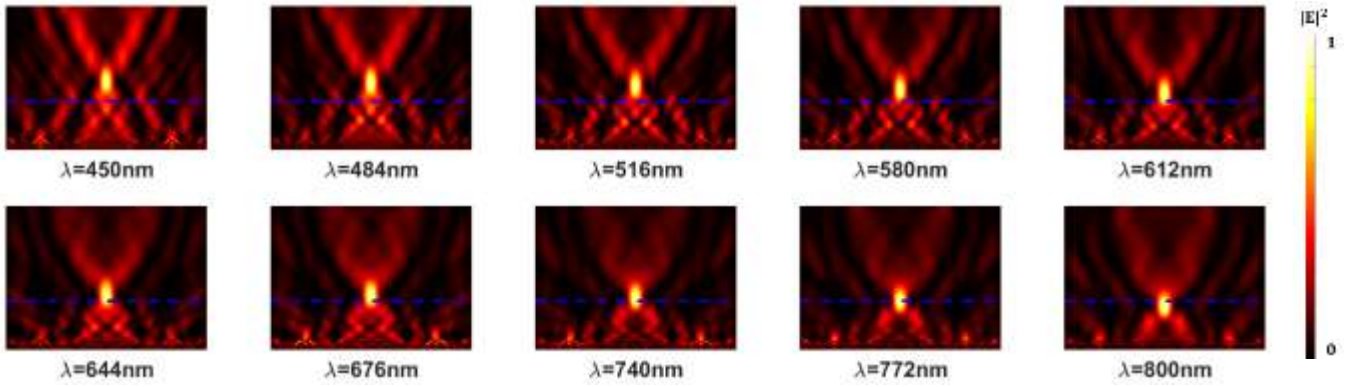

Figure9. The normalized electric field distribution along the simulation area (x-y plane) of the meta-lens with NA =0.8. The blue dashed line represents the focal plane.

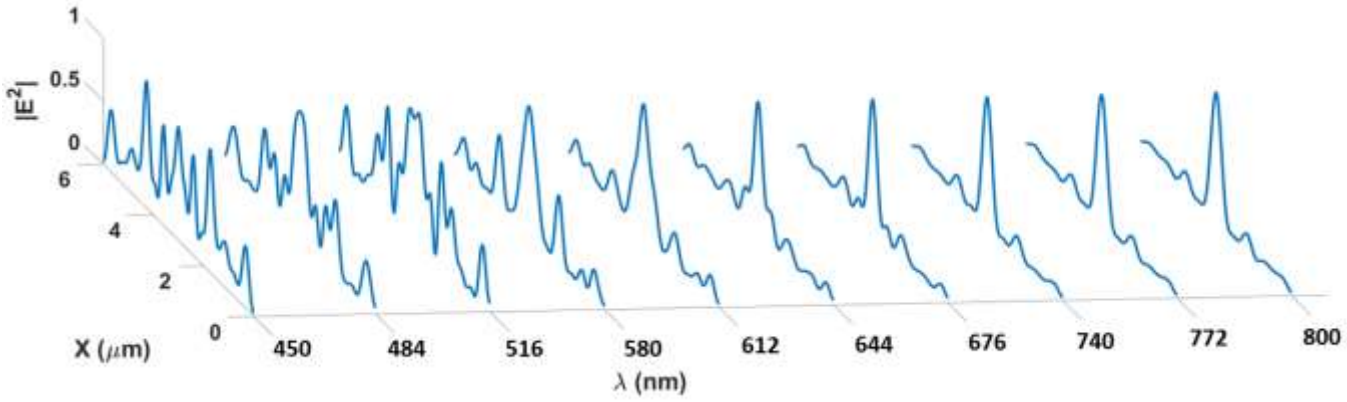

Figure10. The normalized field intensity over the focal plane of the meta-lens with NA = 0.8.

The final design with a very high numerical aperture condition (NA = 0.9) reaches the maximum value of focusing efficiency of 48.67% along the inverse design range in fig. 12(a) and an average value of 25.66%. The focusing efficiency ranges from 5.35% to 48.67% with an average value of 22.14%, while the FWHM in Fig. 12(b) has a minimum value of 202.9 nm, a maximum of 310 nm, and an average value of 207.81 nm. Fig.11 observes the final binarized structure of the design, while fig.13 and fig.14 show the electric field distribution and normalized field over the focal plane, respectively.

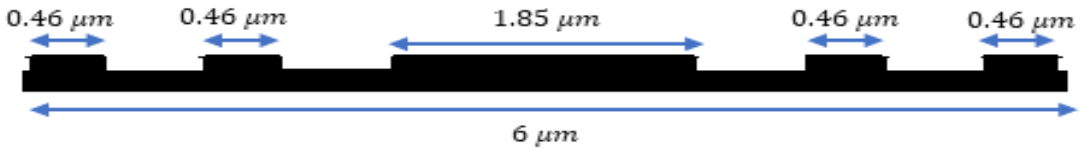

Figure11. The final binary optimized structure of the meta-lens under the numerical aperture condition (NA = 0.9).

(a)

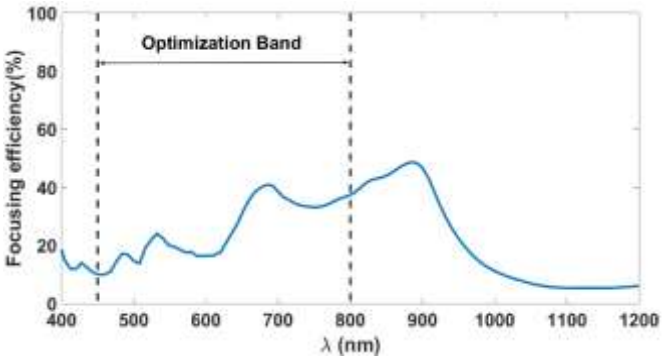

(b)

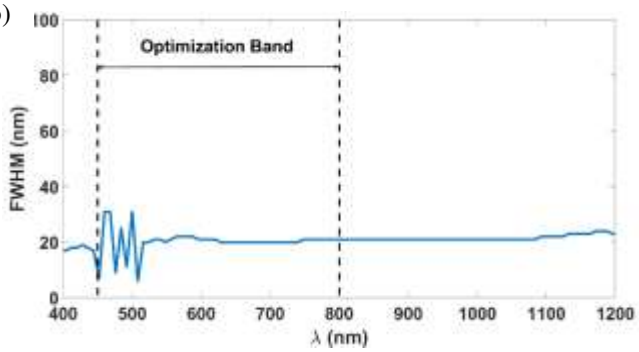

Figure12. (a) Focusing efficiency of meta-lens with NA = 0.9; **(b)** FWHM of meta-lens with NA = 0.9.

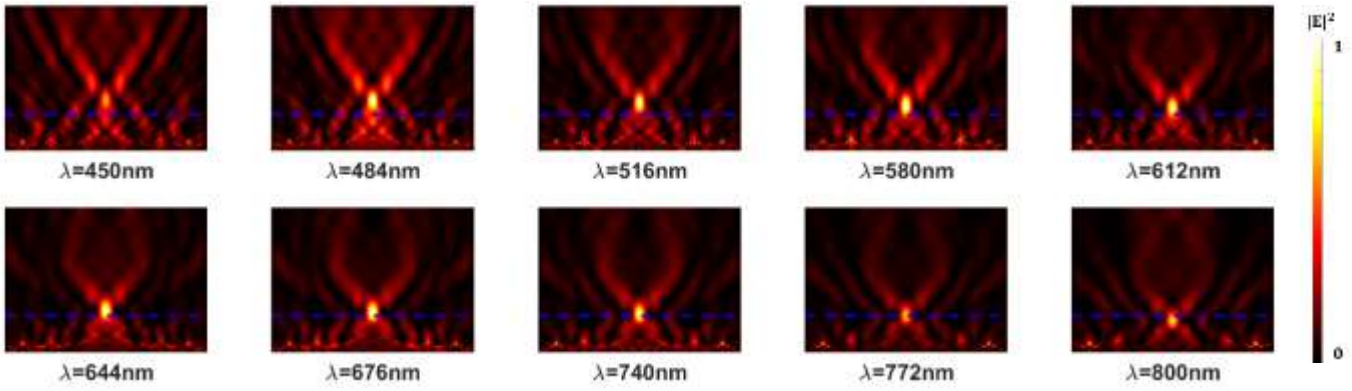

Figure13. The normalized electric field distribution along the simulation area (x-y plane) of the meta-lens with NA =0.9. The blue dashed line represents the focal plane.

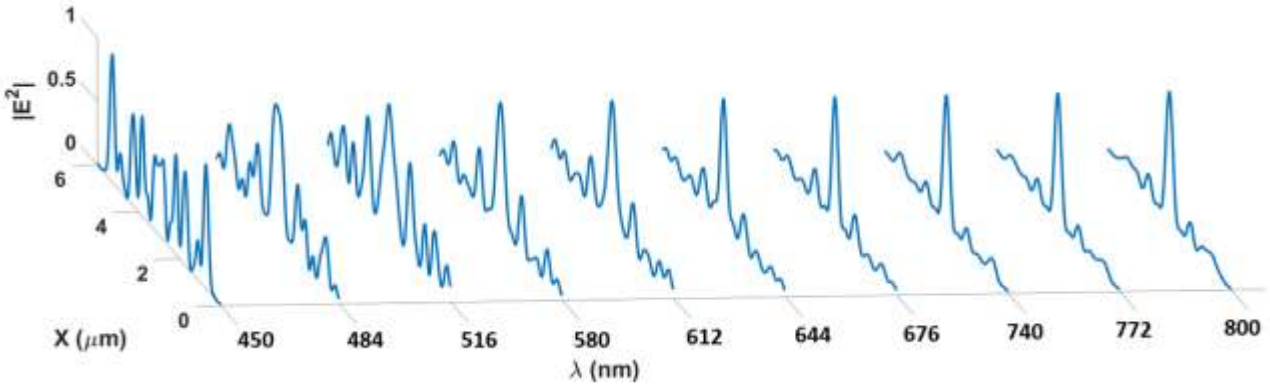

Figure14. The normalized field intensity over the focal plane of the meta-lens with NA = 0.9.

Conclusion

This paper presents a high efficiency broadband achromatic meta-lens based on inverse design with topology optimization. The design depends mainly on the Tio2 material in the wavelength range (400 nm: 1200 nm) for all the band and the inverse design band includes the range (450 nm: 800 nm). The results revealed that the focusing efficiency is very high for all numerical aperture

conditions (NA = 0.7, NA = 0.8, NA= 0.9). The meta-lens leads to many applications and exhibits the potential for multiple optical system designs such as imaging system, biosensing applications, light field camera and spectroscopic system.

Data availability

The datasets used and/or analyzed during the current study available from the corresponding author on reasonable request.

References

1. Abdel-Galil, M., Swillam, M., Ismail, Y. & Khalil, D. High sensitivity refractive index sensing using zone plate metasurfaces with a conical phase profile. *Scientific Reports* **12.** https://doi.org/10.1038/s41598-022-12849-3 (2022).
2. Swillam, M. A. & Helmy, A. S. Analysis and applications of 3D rectangular metallic waveguides. *Optics Express* **18,** 19831. https://doi.org/10.1364/OE.18.019831(2010).
3. Mekawey, H., Ismail, Y. & Swillam, M. Extraordinary Optical Transmission in Silicon Nanoholes. *Scientific Reports* **11.** https://doi.org/10.1038/s41598-021-01068-x (2021).
4. Abdelsalam, M. & Swillam, M. A. Ultra-broadband Mir super absorber using all silicon metasurface of triangular doped nanoprisms. *Scientific Reports* **12.** https://doi.org/10.1038/s41598-022-18817-1 (2022).
5. Abouelatta, M. A., Othman, M. A., Desouky, M., Mahmoud, A. M. & Swillam, M. A. Concentric tubes silicon-based metamaterial structure for mid-IR broadband absorption. *Optics Express* **29,** 41447. https://doi.org/10.1364/OE.441105 (2021).
6. Desouky, M., Mahmoud, A. M. & Swillam, M. A. Silicon based mid-IR super absorber using hyperbolic metamaterial. *Scientific Reports* **8.** https://doi.org/10.1038/s41598-017-18737-5 (2018).
7. Abdel-Galil, M., Ismail, Y. & Swillam, M. Subwavelength focusing in the infrared range using different metasurfaces. *Physica Scripta* **94,** 115511. https://doi.org/10.1088/1402-4896/ab2eb2(2019).
8. Swillam, M. A., Bakr, M. H., Nikolova, N. K., & Li, X.Adjoint sensitivity analysis of dielectric discontinuities using FDTD. *Electromagnetics*, *27*(2–3), 123–140. https://doi.org/10.1080/02726340601166233 (2007)
9. Swillam, M. A., Bakr, M. H. & Li, X. Full vectorial 3-D sensitivity analysis and design optimization using BPM. *Journal of Lightwave Technology* **26,** 528–536. https://doi.org/ 10.1109/JLT.2007.916496 (2008).
10. Swillam, M. *Photonics optimization*. (LAP LAMBERT Academic Publishing, 2013).
11. Lalau-Keraly, C. M., Bhargava, S., Miller, O. D. & Yablonovitch, E. Adjoint shape optimization applied to electromagnetic design. *Optics Express* **21,** 21693. https://doi.org/10.1364/OE.21.021693 (2013).
12. Christiansen, R. E. & Sigmund, O. Compact 200 line matlab code for inverse design in photonics by Topology Optimization: Tutorial. *Journal of the Optical Society of America B* **38,** 510. https://doi.org/10.1364/JOSAB.405955 (2021).
13. Christiansen, R. E. & Sigmund, O. Inverse design in photonics by Topology Optimization: Tutorial. *Journal of the Optical Society of America B* **38,** 496. https://doi.org/10.1364/JOSAB.406048(2021).
14. Chung, H. & Miller, O. D. High-NA achromatic metalenses by inverse design. *Optics Express* **28,** 6945.
15. Lalanne, P. & Chavel, P. Metalenses at visible wavelengths: Past, present, Perspectives. *Laser & Photonics Reviews* **11,** 1600295. https://doi.org/10.1002/lpor.201600295 (2017).
16. El Maklizi, M., Hendawy, M. & Swillam, M. A. Super-focusing of visible and UV light using a meta surface. *Journal of Optics* **16,** 105007. https://doi.org/10.1088/2040-8978/16/10/105007 (2014).
17. Lin, D. et al. Polarization-independent metasurface lens employing the pancharatnam-berry phase. *Optics Express* **26,** 24835. https://doi.org/10.1364/OE.26.024835(2018).
18. Maher, A., Othman, M. A. & Swillam, M. A. High focusing efficiency with high NA broadband Metalens by inverse design with topology optimization. https://doi.org/10.1364/FIO.2022.JW5B.7. *Frontiers in Optics + Laser Science* 2022 (FIO, LS) (2022).
19. Maher, A. & Swillam, M. A. Design of all-dielectric high NA mid infra-red metalens using inverse design and topology optimization. https://doi.org/10.1117/12.2665691. *Metamaterials XIV* (2023).
20. Poon, N. M. & Martins, J. R. An adaptive approach to constraint aggregation using adjoint sensitivity analysis. *Structural and Multidisciplinary Optimization* **34,** 61–73. https://doi.org/10.1007/s00158-006-0061-7 (2006).
21. Lambe, A. B., Kennedy, G. J. & Martins, J. R. An evaluation of constraint aggregation strategies for Wing Box Mass Minimization. *Structural and Multidisciplinary Optimization* **55,** 257–277. https://doi.org/10.1007/s00158-016-1495-1 (2016).
22. Christiansen, R. E., Vester-Petersen, J., Madsen, S. P. & Sigmund, O. A non-linear material interpolation for design of metallic nano-particles using topology optimization. *Computer Methods in Applied Mechanics and Engineering* **343,** 23–39. https://doi.org/10.1016/j.cma.2018.08.034 (2019).

23. Chen, W. T., Zhu, A. Y., Sisler, J., Bharwani, Z. & Capasso, F. A broadband achromatic polarization-insensitive metalens consisting of anisotropic nanostructures. *Nature Communications* **10.** https://doi.org/10.1038/s41467-019-08305-y (2019).

Author contributions statement

M. Swillam suggest and supervised the project. M. Swillam and A.M has performed the theoretical modeling and numerica1 simulations. M. Swillam revised the results. The two authors discussed and edited the manuscript.

Supplementary Files

This is a list of supplementary files associated with this preprint. Click to download.

- Appendix.docx